Thermodynamic Scaling of Extreme Daily Precipitation over the Tropical Ocean from Satellite Observations

Victorien de Meyer, Rémy Roca

Journal of the Meteorological Society of Japan

EARLY ONLINE RELEASE

The DOI for this manuscript is
DOI:10.2151/jmsj.2021-020
J-STAGE Advance published date: January 14th, 2021

Thermodynamic scaling of extreme daily precipitation over the tropical ocean from satellite observations

Victorien De Meyer[1] and Rémy Roca[1]

[1]Laboratoire d'Études en Géophysique et Océanographie Spatiales (Université de Toulouse III, CNRS, CNES, IRD), Toulouse, France

Submitted to

The Special Edition on "Global Precipitation Measurement (GPM): 5th Anniversary"

in Journal of the Meteorological Society of Japan (JMSJ)

29 July 2020

Revised 1

6 October 2020

Revised 2

3rd December 2020

Key words: extreme precipitation, tropical ocean, satellite observations, scaling

Corresponding author address: Dr Rémy Roca, Observatoire Midi-Pyrénées, Laboratoire d'Etudes Géophysiques et d'Océanographie Spatiales, 14 Avenue Edouard Belin 31400 Toulouse, France. Email: remy.roca@legos.obs-mip.fr

Abstract

Extreme precipitation theory has been matured over the last decade and stipulates that the intensity of the extreme precipitation scales with the surface humidity. Surface humidity changes can further be approximated by the surface temperature changes. The analytically derived scaling coefficient based on the Clausius-Clapeyron derivative is ~6%K^{-1} in the tropics. While frequently confronted with observations over land, the theory has so far only been marginally evaluated against precipitation data over the ocean. Using an ensemble of satellite-based precipitation products and a suite of satellite-based SST analysis all at the 1°-1day resolution, the extreme scaling is investigated for the tropical ocean (30°S-30°N). The focus is set on the robust features common to all precipitation and SST products. It is shown that microwave constellation-based precipitation products are characterized by a very robust positive scaling over the 300 to 302.5K range of 2-day lagged SST. This SST range corresponds to roughly 60% of the tropical precipitation amount. The ensemble mean scaling varies between 5.67%K^{-1} +- 0.89%K^{-1} to 6.33%K^{-1} +- 0.81%K^{-1} depending on the considered period and is found very close to the theoretical expectation. The robustness of the results confirms the fitness of the current generation of constellation-based precipitation products for extreme precipitation analysis. Our result further confirms the extreme theory for the whole tropical ocean. Yet, significant differences in the magnitude of the extreme intensity across the products prompts the urging necessity of dedicated validation efforts.

1 INTRODUCTION

The energy and water exchanges within the Earth system are related to the major feedback processes responsible for the fate of the Earth climate under increasing greenhouse gases concentrations (Stephens et al. 2020). The second principle of thermodynamic and the Clausius Clapeyron law indeed dictate that water vapor in the atmosphere increases at a rate of 6-7% with each degree warming which is at the heart of the strongly positive water vapor feedback. The increased loading of water vapor in the atmosphere has a strong impact on both the mean precipitation (Stephens and Ellis 2008) and the distribution of its extreme (Trenberth 1999).

Theory for extreme precipitation dependence on surface temperature has indeed matured significantly over the last decade and a physically based framework is now well established (Gorman and Schneider 2009; O'Gorman 2015; Fischer and Knutti 2016). Yet cloud resolving model idealized simulations over tropical oceans exhibit diverging sensitivities and a number of open questions remains in the tropics (Muller and Takayabu 2020). Land based studies using conventional precipitation observations over tropical land also suggests contrasting results (Westra et al. 2014). Recent investigations using satellite observations nevertheless have identified robust extreme precipitation regimes in agreement with the theoretical expectations from thermodynamics (Roca 2019). Over the ocean, on the other hand, the scarcity of conventional in-situ precipitation observations (Serra 2018) precluded much investigations of the scaling of extreme precipitation with surface temperature with notable exceptions.

Using early instantaneous satellite observations from Special Sensor Microwave/Imager (SSM/I) and monthly SST from Hadley Centre Sea Ice and Sea

Surface Temperature data set (HadISST) (Rayner et al. 2003), Allan and Soden (2008) calculated the rate of change of 2.5°x2.5° daily precipitation to tropical mean monthly SST anomalies. Extreme precipitation shows a scaling ranging from slightly above, to much larger than their value derived from the Clausius-Clapeyron response depending on the base line for the anomaly computations. The analysis further pointed out systematic underestimation of the response of the climate models prompting for a more in-depth analysis of the behavior of the extremes over the oceans. The use of tropical mean SST anomaly nevertheless prevents from further addressing the processes at play.

More recently, using the OceanRAIN dataset of ship based disdrometer precipitation measurements (Klepp et al. 2018), the scaling of instantaneous (at 1 minute scale) extreme precipitation to the *local simultaneous* SST has been revisited for the global ocean (Burdanowitz et al. 2019). The disdrometer data exhibits a single increasing regime of the 99th percentile with local SST. The scaling is computed by pooling available data over a large range of SST (0°C-30°C) and is shown to vary between 6%K^{-1} and ~9%K^{-1} depending on the regression technique used. Yet, the small sample of the ship-based measurements prevents a definitive conclusion and the relative role of the convective dynamics and of thermodynamics remains to be clarified at these scales.

In summary, many observation-based assessments of the scaling theory have taken place under continental conditions while model-based assessments are performed under oceanic conditions. In comparison, the tropical ocean so far benefited from very few observationally based investigations. In this paper, we propose to improve this situation by pooling recent satellite observations at the 1°x1° daily scale of both precipitation and surface temperature all over the tropical oceans.

Over the ocean, the evaluation of these satellite-based products is generally performed using the few available data from buoys networks (Wu and Wang 2019), atolls rain gauges observations (Greene et al. 2008) or island based radar measurements (Henderson et al. 2017). More recently, the release of a new ship-based disdrometer measurements database (Klepp et al. 2018) provides a complementary reference dataset over some commercial ship routes and research vessel campaigns. For large space and time scales, consistency analysis can be performed through water and energy budget conservation analysis (L'Ecuyer et al. 2015). As a consequence of these limited verification references, compared to land, the capability of these satellite-based products to describe the precipitation field is generally not very well documented (Sun et al. 2018), not mentioning under the extreme rainfall conditions. Instead of elaborating on the difficulty to quantify the accuracy of the products, the rationale of this study is to focus on the robustness of the analysis across many satellite products to investigate the thermodynamic scaling of extreme precipitation with sea surface temperature.

Section 2 introduces a number of satellite-based products of both precipitation and SST and details the methodology followed in this study. Section 3 is dedicated to the presentation of the results and a sensitivity of the results to various assumptions. Finally, a summary and discussion section ends the paper.

2 DATA AND METHOD

2.1 PRECIPITATION

The list of the various products under consideration is provided in Table 1. All the datasets are used at the same 1°x1° daily resolution over the 30°s-30°n region and originate mostly from the Frequent Rainfall Observations on GridS (FROGS) database (Roca et al. 2019) under the DOI https://doi.org/10.14768/06337394-73A9-407C-9997-0E380DAC5598. While the products share some of the raw satellite observations, they differ in many aspects that can influence their capability of describing precipitation. They are built from different instantaneous rain rates algorithms. The daily accumulation from the various products further benefits from different sampling from single or multiple platforms, from infrared and/or microwave imagers and/or sounders. Finally, some products also incorporate in-situ corrections.

The Global Precipitation Climatology Project (GPCP) is a pioneer effort to provide satellite based precipitation estimates globally (Huffman et al. 1997). We here use the one degree daily climate data record v1.3 detailed in Huffman et al. (2001). The GPCP 1 degree-daily (1DD) product relies on a single microwave platform, infrared measurements and the GPCC analysis over land. The daily estimates are adjusted as to mimic the GPCP monthly product when aggregated over a month. Note that the GPCP monthly product is used in various other products as an adjustment reference. The Precipitation Estimation from Remotely Sensed Information using Artificial Neural Networks (PERSIANN) family of products has various incarnations. We here use the climate oriented product the Climate Data Record (CDR) version, also known

as PERSIANN-CDR v1 (Ashouri et al. 2015). PERSIANN is a based on infrared imagery and it is adjusted to the GPCP monthly mean. It can be seen as an alternative downscaling of the GPCP monthly data to that of GPCP 1DD. The National Oceanic and Atmospheric Administration (NOAA) Climate Prediction Center (CPC) morphing technique (CMORPH) satellite precipitation estimates (Xie et al. 2017) rely on the constellation of both microwave imagers and sounders and infrared derived cloud motion winds. The blending of the various data is performed thanks to a Kalman filter (Joyce and Xie 2011). Over the ocean, the product is adjusted onto the GPCP accumulations. Compared to buoys, CMORPH under (over) estimate rainfall over the Atlantic (Pacific) ocean (Wu and Wang 2019). The Tropical Rainfall Measuring Mission Multisatellite Precipitation Analysis (TMPA) product is a widely used dataset that combines radar, infrared, microwave imagers and sounders satellite observations (Huffman et al. 2007). Version 7 is used here. Over tropical Atlantic (Pacific), the TMPA product shows overall under(over)-estimation (Wu and Wang 2019). Over the northern Indian ocean, the TMPA product generally overestimated precipitation compared to the buoys but underestimates heavy precipitation events over 100mm/d (Prakash and Gairola 2014). Note that earlier investigation noted that TMPA monthly means are similar to the GPCP product over tropical ocean (Huffman et al. 2007). The Hamburg Ocean-Atmosphere Parameters and Fluxes from Satellite Data (HOAPS) product provide a satellite based suite of fresh-water budget parameters including precipitation over sea-ice-free ocean surface (Andersson et al. 2010). This microwave only product relies on multi-platforms inter-calibrated measurements from SSM/I and Special Sensor Microwave Imager Sounder (SSMIS) (Fennig et al. 2020). Version 3.2 of the precipitation product is used (Andersson et al. 2014). When compared to the oceanRAIN in situ

data, HOAPS instantaneous rain rate underestimates intensity in the intertropical convergence zone especially for high rain rate but at the same time, the HOAPS retrieval overestimates the occurrence of precipitating cases (Bumke et al. 2019). The Tropical Amount of Rainfall with Estimation of ERors (TAPEER) algorithm makes use of geostationary infrared imagery together with microwave imager instantaneous rain rates estimates plus the SAPHIR sounder to estimate daily-precipitation accumulation (Roca et al. 2020). The addition of the Megha-Tropiques platform in the constellation is shown to improve the product compared to imagers only implementation (Roca et al. 2018).The recently released TAPEER product has been extensively evaluated over West Africa (Gosset et al. 2018) but is not well characterized over the tropical ocean yet. The Global Satellite Mapping of Precipitation (GSMaP) product provides high-resolution precipitation estimations using satellite observations from multiple platforms (Kubota et al. 2020) . This product is mainly based on the microwave estimation of rainfall from a suite of microwave imagers and sounders. The microwave instantaneous rain rate estimates (Aonashi et al. 2009; Shige et al. 2009) are propagated based on cloud motion wind vectors originally derived from IR geostationary imagery (Ushio et al. 2009). Here the near real time version 6 product is used. The Integrated Multi-satellite Retrievals for Global Precipitation Measurement mission (GPM) (IMERG) is developed at NASA based on infrared observations and on both microwave imagers and sounders data (Huffman et al. 2020). It takes advantage of the TMPA product, the CMORPH-Kalman Filter approach (Joyce and Xie 2011) and the PERSIANN-Cloud Classification System algorithm (Hong et al. 2004). The most recent v6 release of the final run product is used. Previous evaluation efforts showed that the older version (V4) overestimates rain-rates compared to buoys observations at hourly 0.1°x0.1° scale over the north

187 Indian Ocean (Prakash et al. 2017). Version 5 daily 1°x1° estimates are shown to
188 underestimate the OceanRAIN measurements on average that is likely due to the
189 inclusion of very light rain rates in the statistics (Khan and Maggioni 2019). While
190 IMERGv5 has similar biases with respect to in-situ data than CMORPH and TMPA, it
191 overall better performs in the estimation of the mean value with the exception of the
192 Atlantic ocean regime over 4mm/d where the product is shown to significantly
193 underestimate precipitation (Wu and Wang 2019) . Version 6 of the product benefits
194 from a refined intercalibration procedure and better interpolation between the
195 platforms that show improvements on some metrics (Tan et al. 2019) and should
196 also reflect on these prior evaluations. The Multi-Source Weighted-Ensemble
197 Precipitation (MWSEP) is a product that corresponds to a pragmatic approach that
198 average existing products to provide a best estimate. Over land an optimization
199 method based on hydrological modelling and observed stream-gauges data is used
200 (Beck et al. 2017). Over ocean, a merging procedure is also followed. The various
201 source of precipitation used encompass satellite-based products, rain gauge
202 measurements and reanalysis results. We use here Version 2.2 (Beck et al. 2019).
203 From the 2000 on-wards, MSWE estimates over the tropical ocean are weighted
204 much more towards satellite products than reanalysis. CMORPH, GSMaP-MKV v5
205 and TMPA v7 RT are blended in MSWE. Note that over ocean TMPA v7 RT and
206 TMPA v7 are similar and only differ over land. The geographical distribution of the
207 99^{th} percentile of 3-hourly precipitation of MSWEP2.2 is very close to that of
208 CMORPH over the tropical ocean (Beck et al. 2019).

209

210 The resulting variety of precipitation distribution from these nine products is illustrated
211 in Figure 1. The two products that do not rely on the microwave constellation (GPCP

and PERSIANN) exhibit strongly decreasing occurrence with the daily precipitation amount; GPCP not having values above 170 mm/d. The TAPEER product exhibits systematic significant underestimation of the probability of the largest rain accumulation compared to other microwave-based products. This is likely due to the relative lack of light rain situations (Roca and Fiolleau, 2020). Note that the TAPEER product is also only available for a limited time period. Owing to their outlier distribution and documented biases, those three products are not considered in the following. The figure further reveals two clusters of products showing both the occurrence declining smoothly exponentially towards the very high daily precipitation accumulation. The first cluster is composed of CMORPH, TMPA and MSWEP. The members of this cluster are very close with MSWEP being built from CMORPH and TMPA. Both CMORPH and TMPA further share the same adjustment to the common reference of GPCP pentads over the ocean. The second one includes GSMaP, HOAPS and IMERG that do not share much in terms of algorithms, methods and input data. While the two clusters show a similar distribution up to 100 mm/d, above that threshold, the first cluster systematically underestimates the occurrence compared to the second cluster. This is consistent with previous analysis that indicate that the climatological mean behavior of the products is a poor predictor of the products extreme precipitation (Masunaga et al. 2019). The first cluster products have further been shown to underestimate the intense rain rates compared to buoys (Prakash and Gairola 2014; Wu and Wang 2019) that could be related to their difference with the second cluster.

2.2 SEA SURFACE TEMPERATURE

Satellite based SST products readily provide estimations of the foundation SST, defined as the ocean temperature at a depth of ~1 meter, below the diurnal layer, at

high space and time resolution over a long temporal record. Most of the products rely on optimal interpolation techniques to merge various satellites observations with in-situ measurements. While such products have a well characterized accuracy under clear sky conditions of ~0.5K (Donlon et al. 2012), their representativity under (extreme) rainfall conditions is not well documented. Indeed, the cloudiness associated with the rainfall prevents the use of infra-red measurements and the microwave signal, while of help in cloudy but non-precipitating cases, is altered by rain drop emission during the heavy precipitation situations, also preventing SST estimation in this case (Wentz et al. 2000). As a consequence, the SST estimates under precipitating conditions mainly rely on the result of the optimal interpolation method and are smoothed over several days and a large distance. In the following, we interpret these fields as “synoptic” SST and assess whether such synoptic SST are a good and robust proxy for the thermodynamics of the extreme precipitation events over the ocean. A suite of 3 products is used to evaluate the sensitivity of the scaling to the input data and to the optimal technique implementation and are summarized in Table 2. All SST products have been regridded at a daily 1°x1° resolution over the 30°S-30°N region to match the precipitation data using a simple conservative averaging procedure.

The Operational Sea Surface Temperature and Ice Analysis (OSTIA) (Donlon et al. 2012) product provides a global foundation SST field derived from satellite observations in the microwave (2 platforms) and in the infrared (6 platforms) and in-situ measurement at 1/20° and daily resolution since 2007. The analysis is a multi-scale optimal interpolation using a three days assimilation window centered on the day of the analysis and the background field is the analysis of the previous day. The

error correlation length scale used in OSTIA in the tropics is around 100 km. The product Optimum Interpolation Sea Surface Temperature (OISST) (Banzon et al. 2016) uses IR measurements from the Advanced Very High-Resolution Radiometer (AVHRR) instruments on board the NOAA satellites since 1981. The interpolation method is similar to that of OSTIA. The error correlation length scales in the tropics are about 150-200km and 3 days. The nominal resolution is daily at 0.25°. Version 2 of OISST is used here. Finally, the microwave (MW) optimally-interpolated (OI) SST product from Remote Sensing Systems (Gentemann et al. 2010) is used. As some rain-contaminated SST estimate may persist in the microwave derived dataset, a stringent quality control is performed to prevent potentially biased SSTs retrievals. The error correlation scales used are of 100 km and 3 days, the background field is the analysis of the previous day and the SST represents a foundation SST remapped at a daily 1°x1° resolution. This product is referred to as OIRSS in the following.

2.3 METHOD

1) Background on the theory

The background on the scaling of extreme precipitation with surface temperature has been detailed and reviewed in various publications (O'Gorman 2015; Allan and Liu 2018; Roca 2019; Muller and Takayabu 2020) and is only briefly summarized below. Based on the dry static energy budget of the atmosphere (Muller et al. 2011), the rate of extreme precipitation in the tropics can be expressed as follow:

$$P_e = \epsilon \int \rho\omega \left(-\frac{\partial q_{sat}}{\partial z}\right) dz, \quad (1)$$

where ϵ depicts a precipitation efficiency, ρ the mean density profile, ω the vertical velocity, q_{sat} the saturation mixing ratio and with the integral taken from the surface

to the tropopause. Furthermore, the fractional change of extreme precipitation $\frac{\delta P_e}{P_e}$ with warming highlights three contributions, that is the change in microphysics related to the efficiency term, the change in dynamics through $\rho\omega$ and the change in thermodynamics through $\frac{\partial q_{sat}}{\partial z}$. At the daily 1°x1° scale, with the assumption that the related change of the dynamic and efficiency contributions remain low with warming and by neglecting the vertical variations in ω, the scaling of extreme precipitation becomes (Muller et al. 2011)

$$\frac{\delta P_e}{P_e} \approx \frac{\delta q_s^{surface}(T)}{q_s^{surface}(T)}. \quad (2)$$

It points out that the change in precipitation extremes is expected to be more related to the surface conditions rather than to the column integrated, and at a rate following the rate of increase of $q_s^{surface}$ with temperature, that is the Clausius-Clapeyron rate. In typical tropical sea surface conditions, the expected value ranges between 5.5 and 6.5%K^{-1}.

2) Methodological aspects

Extreme daily precipitation is characterized using high percentiles of the wet-days (P>1mm/d) distribution. This index is chosen over others (Zhang et al. 2011) due to its relevance for scaling investigations (Schär et al. 2016). The scaling of the precipitation extremes with the sea surface temperature is calculated using the binning method which is well suited to our investigation given the large number of available observations (Roca 2019). Indeed, for each 0.5K degree SST interval, precipitation data from the whole tropical ocean are pooled together and the 99.9th percentile of the precipitation distribution is estimated. Then after identifying a

relevant regime, linear regression (in the logarithm space) is used to compute the scaling factor defined as the rate of change of the 99.9th percentile with sea surface temperature.

3) Sensitivity studies for robustness determination

In order to identify the robust aspects of the thermodynamic scaling estimation using satellite observations, we perform a sensitivity study in complement to the use of various precipitation and SST products. We explore how the timing between the SST and the precipitation influences the scaling and how the overall statistical analysis is sensitive to the selected period.

As already well explored for continental cases (e.g., Bao et al. 2017) intense precipitation events can strongly alter the surface heat budget and the surface temperature. The strong gust and downdrafts associated with deep convection result in a lower surface temperature compared to the no rain case (Lafore et al. 2016). As a result, the surface conditions may not represent the large-scale environment of the event but are impacted by the event itself. As discussed above, the synoptic SST products assimilation scheme prevents these impacted surface conditions to be used in the estimation, yet the risk to misattribute a rain event to a given temperature range because of this coupling is unclear. As a mean to assess the impact on our findings, the timing of the association between SST and the precipitation event is varied from simultaneous and lagged up to two days before.

The constellation-based precipitation products are characterized by a changing configuration of the constellation over the last two decades depending on the availability of microwave imagers and sounders that could influence their capability to monitor steadily the precipitation in the tropics (Roca et al. 2020).The SST products are also sensitive to the availability of the microwave imagers and the infrared radiometers. The availability of these platforms since 2001 is summarized in Figure 2. The baseline period for our investigation spans 2007-2017 which is the longest period share by all SST products. It corresponds to the homogeneous cycle of production of OSTIA (Donlon et al. 2012) and to the start of the systematic use of two AVHRR instruments for the OISST product (Banzon et al. 2016). Two other different periods are considered. The first one is longer, extending back in time until 2001 for which OIRSS and OISST are available and correspond to the availability of the GSMaP precipitation product. During the 2001 to 2007 era, the microwave imagers fluctuate from 4 to 6 platforms and the sounders from 2 to 4 while the IR radiometers increases from 1 to 3. These constellation configurations are all less populated than the forthcoming period post 2007 and the products are associated with less sampling than during the 2007-2017 that could impact our analysis. The second period is a shorter one and corresponds to a precipitation data rich era that includes the Megha-Tropiques operations (Roca et al. 2018) and partly includes the TRMM and GPM platforms along with the SSM/I and SSMIS platforms. This era is characterized with up to 14 microwave sensors operating simultaneously. The use of three periods of 18, 11 and 5 years, respectively also permits to assess the sensitivity of the estimation of the extreme percentile of the precipitation distribution.

3 RESULTS

3.1 SIMULTANEOUS ANALYSIS

Figure 3 shows the scaling of the 99.9th percentile as a function of the simultaneous SST from the OSTIA product for the 6 constellation-based products. The two clusters of precipitation products previously identified are shown as well. The low cluster 99.9th percentile ranges from 120 to 150 mm/d while the high one spans 170 to 240 mm/d. There is roughly a factor of two among the least value of CMORPH at 297K and the highest one of IMERG at 302.5K. The dependence of the high percentile to the SST is characterized by three regimes. Up to 300.25K, the products do not exhibit any robust behavior. GSMaP is mainly increasing over this SST range, while HOAPS extremes decrease; the other products rather show no sensitivity to the SST. This regime accounts for only 19% of the total tropical precipitation accumulation. The second regime spans SST from 300K up to 302.5K and is characterized by an increase of all the products. Almost 56% of the total rainfall belongs to this regime. For the last regime, above 302.25K and corresponding to 25% of the total rainfall amount, the precipitation products show a robust decrease of the value of the high percentile. For the second regime, the ensemble mean of the scaling is ~5%K^{-1} with a small coefficient of variation of around 10% and range from 4.21 to 5.75 %K^{-1} (Table 3a). A robust scaling, close to the Clausius Clapeyron, is found in this case.

The replacement of OSTIA by OISST does not change the regime decomposition much (not shown) but the ensemble scaling over the regime 2 is much smaller (3.4%K^{-1}) and spreads almost twice much more (Table 3b). The use of the OIRSS data, on the other hand, drastically alters the picture with no well-defined regimes at all. Over the previous SST range of regime 2, the ensemble scaling is even slightly

379 negative (-0.45%K^{-1}). The scaling obtained from simultaneous measurements of
380 precipitation and surface temperature are hence not robust to the selection of the
381 SST products.

382 ## 3.2 LAGGED ANALYSIS

383 The lagged analysis using the SST of the day before the precipitation does not
384 change much the overall picture (not shown). Quantitatively, the ensemble mean of
385 the scaling slightly increases to 5-6%K^{-1} with a coefficient of variation less than 11%
386 for all the OSTIA and OISST products (Table 3a and b). The OIRSS product now
387 exhibits a scaling of 4.4%K^{-1} +- 0.6%K^{-1} value. On the other hand, the lagged
388 analysis at two days before confirms the previously identified low and high
389 precipitation products clusters and reveals a very robust pattern across the SST
390 products. Figure 4 confirms the relevance of the range of the scaling regime identified
391 for OSTIA for all the SST products. The sensitivity of the selection of the upper bound
392 303K instead of 302.5K (not shown) does not modify the values significantly. With a 2
393 days lag, the ensemble mean scaling is very similar for each SST product: 5.9, 5.9
394 and 6.0 %K^{-1} for OSTIA, OISST and OIRSS, respectively. The ensemble variance is
395 also similar among the products at around 10% (or 0.65%K^{-1}). The multi precipitation
396 products and multi-SST products ensemble of 18 combinations statistics reads
397 5.93%K^{-1} +- 0.60%K^{-1}. The “cold” regime with SST < 300K remains non-robust at
398 day-2 lag, with the precipitation products not agreeing on the sensitivity of the 99.9th
399 percentile to the SST. The warm regime with SST ≥ 302.5K is characterized by a
400 robust behavior of the precipitation products does not appear robust to the SST
401 selection. The marked decrease of the extreme in OSTIA after 302.5K is rather
402 associated with a smooth, steady evolution for OISST and OIRSS. Note that the
403 GSMaP product, unlike any other product, indicates a CC-like positive scaling over

most of the cold regime. This unique feature deserves further attention and will be investigated in the future.

3.3 SENSITIVITY TO THE SELECTION OF THE PERIOD

The analysis for the longer period is summarized in Figure 5. The “cold” regime results still hold in this case although its upper limit can be revised to 299.5K. The “warm” regime is now more robust among the SST products but the 302.5K limit is less clearly marked than for the 2007-2017 period. The values of the 99.9th percentile is slightly higher for all precipitation products compared to the previous period. The scaling over the 300K-302.5K regime shows a smoother sensitivity than before with an ensemble mean value of 4.3 and 5.3 $\%K^{-1}$ for the two SST products (Table 3b and c). When the range is slightly adjusted to 299.5K and 302.0K, the regime corresponds to 45% of the total precipitation and the scaling now reads 5.65 and 5.69$\%K^{-1}$ for OISST and OIRSS, respectively. In this case, the spread of the ensemble scaling for OISST is diminished to ~17% instead of 24% (Table 3b) and remains the same at ~15% for OIRSS. The ensemble of 12 combinations for all SST and precipitation products in this case is 5.67$\%K^{-1}$ +- 0.89$\%K^{-1}$.

Figure 6 confirms the three regimes delineation for the shorter period. The magnitude of the extreme precipitation is close to that of the 2001-2017 period. The ensemble mean scaling is slightly larger and now ranges between 6.0 and 6.8 $\%K^{-1}$ while the 18 combinations for all SST and precipitation products is 6.33$\%K^{-1}$ +- 0.81$\%K^{-1}$, also in close agreement with the theoretical expectation. Owing to its availability over that period, the TAPEER products is also shown for the sake of completeness but it is not included in the ensemble statistics. It is in line with the other products, although with

a much lower magnitude of the p99.9 marker as expected from Figure 1. Yet the scaling mean value is ~5.1%K^{-1} which is slightly less than for the other products.

4 SUMMARY AND DISCUSSION

The objective of this study is to explore the scaling of extreme precipitation with surface temperature over the tropical oceans. The pooling of data originating from an ensemble of 6 constellation-based precipitation products reveals two clusters of products that differ in terms of magnitude of the extreme daily accumulation. The difference between the low cluster (MSWE, TMPA and CMORPH) and the high cluster (HOAPS, GSMaP and IMERG) spans roughly a factor of two at the most. No such clustering is found over land, likely due to the inclusion of rain gauges in most of the products (Roca 2019; Masunaga et al. 2019). While, buoy-based comparison suggests the low cluster products indeed underestimate intense precipitation intensity, no definitive argument yet permits to prefer one cluster from the other. Despite this magnitude difference, the present results highlight a very robust behavior of the satellite products extreme precipitation with respect to the SST. The explanation for the individual product similarities and differences would require a dedicated study and is out of the scope of the present work that focus on the precipitation products ensemble robust features.

The timing of the SST-precipitation relationship has also been explored and it is shown that the two days lagged investigation exhibits robust regimes across the SST products. This is likely due to the use of the SST analysis that blends data over 3 days and ~100km to provide an SST estimate under precipitating conditions. Our

study confirms the fitness for purpose of these analyzed SST for precipitation related investigations. Specifically, the two days lagged analysis identifies three distinct regimes:

A “cold” regime with SST < 300K that corresponds to ~19% of the total tropical precipitation amount. In this case, while the results are not sensitive to the SST product selection, nor to the timing of the precipitation-temperature association nor the length of the record, the various precipitation products exhibit inconsistent behaviors. The lack of robustness of the results might be due to some structural errors in the precipitation retrievals and/or to the weak data sampling preventing a robust estimation of the high percentile of the precipitation distribution. The 99^{th} percentile (not shown), that ranges between 60 and 100mm/d over the cold regime, is less sensitive to the data sampling than the 99.9^{th} percentile and shows a lack of sensitivity that is more reproductible among the products but for HOAPS that still differs from the other five products.

A “warm” regime with SST > 302.5K corresponding to ~25% of the total precipitation amount, is characterized by a systematic decrease of the values of the 99.9^{th} percentile from 302.5K to the warmest SST under considerations. This warm regime is also observed over land (Roca 2019) and is usually attributed to relative humidity limited conditions at warm surface temperature that decrease the intensity of extreme precipitation over these semi-arid areas. Decrease in the wet-days duration for this regime has also been identified as a key mechanism over mid-latitudes land conditions (Utsumi et al. 2011). Further analysis is needed to assess whether these

very high SST are associated with large scale subsidence and simultaneous relatively dry boundary layer that could impact the intensity and/or the duration of the precipitation events and explain the decreasing trend. Burdanowitz et al. (2019) do not report any such decreasing regime when analyzing instantaneous disdrometer derived precipitation rate from ship data. They attribute this departure from the behavior of the continental extreme to the absence of decreasing event duration in this regime. Yet their analysis is restricted to 1K SST bin up to 303K, and hence would miss the warm regime identified here. Furthermore, our study shows that the use of simultaneous SST is detrimental to the scaling computation. It is likely that using a time lagged analysis of the instantaneous precipitation scaling over an extended SST range would permit to better delineate the various regimes relevant for that instantaneous scale.

The third regime which we call the « Clausius-Clapeyron » regime is ranging from 300K to 302.5K and includes almost 56% of the total precipitation amount. It is characterized by a steady increase of the extremes with surface temperature. This regime is robust to the precipitation product, to the SST product and to the length of the record. When simultaneous SST data are used, the scaling is diminished but for OIRSS where it simply does not exist. The one day lagged scaling results are robust to the SST product selection and lead to a scaling around $5.17\%K^{-1}$ +- $0.85\%K^{-1}$. The two days lagged scaling value ranges from $5.67\%K^{-1}$ +- $0.89\%K^{-1}$ for the 2001-2017 period to $6.33\%K^{-1}$ +- $0.81\%K^{-1}$ for 2012-2016 for all the SST and precipitation products considered here. While the actual, direct validation or evaluation of the representation of intense rain accumulation in these products remains challenging, their common and physically sound behavior indicates that the products are fit for

exploring the extreme precipitation over the ocean. The robustness of the scaling analysis across the satellite precipitation products is further very close to the theoretical expectation for the thermodynamic scaling of ~6%K^{-1}. This gives us even more confidence in this generation of satellite precipitation products at the 1° 1-day resolution over the ocean. The frequency of occurrence of the precipitation greater than the 99.9th percentile and surface conditions corresponding to the Clausius Clapeyron regime have been mapped in Figure 7. The figure points out that this regime is not associated with the climatological ITCZ location as previously noted (Masunaga et al. 2019). On the other hand, it is associated with the known climatological rainfall maxima, off the Colombian Coast and in the northern Bay of Bengal and also seems to align with the climatological distribution of cyclones occurrence in the East Pacific, West Atlantic, South Indian Ocean and China sea.

An avenue for further research lies in identifying the contribution of the organized convection to the scaling physics (Pendergrass 2020; Muller and Takayabu 2020; Roca and Fiolleau 2020). Our results further prompt for a dedicated investigation of the contribution of the cyclone precipitation to the scaling physics that is so far not much promoted. Our results also suggest that community efforts, possibly under the umbrella of the International Precipitation Working Group (Levizzani et al. 2018) and the GEWEX/WCRP core-project, are needed to further characterize the absolute accuracy of precipitation products over the ocean and clarify which clusters of products is to be understood as a reference, if any.

5 ACKNOWLEDGEMENTS

This study benefited from the IPSL mesocenter ESPRI facility, which is supported by CNRS, UPMC, Labex L-IPSL, CNES and Ecole Polytechnique. The authors acknowledge the CNES and CNRS support under the Megha-Tropiques program. They also thank Dr T. Fiolleau for helpful discussions and Dr. M. Schröder for his help with the HOAPS dataset.

6 REFERENCES

Allan, R., and C. Liu, 2018: Evaluating Large-Scale Variability and Change in Tropical Rainfall and Its Extremes. *Tropical Extremes: Natural Variability and Trends*, V. Vuruputur, J. Sukhatme, R. Murtugudde, and R. Roca, Eds.

Allan, R. P., and B. J. Soden, 2008: Atmospheric warming and the amplification of precipitation extremes. *Science (80-.).*, **321**, 1481–1484, https://doi.org/10.1126/science.1160787.

Andersson, A., K. Fennig, C. Klepp, S. Bakan, H. Graßl, and J. Schulz, 2010: The Hamburg ocean atmosphere parameters and fluxes from satellite data-HOAPS-3. *Earth Syst. Sci. Data*, **2**, 215–234, https://doi.org/10.5194/essd-2-215-2010.

Andersson, A., M. Schröder, K. Fennig, J. Kinzel, S. Bakan, and C. Klepp, 2014: Ocean Surface Freshwater Fluxes from the HOAPS Satellite Climatology. 2014.

AONASHI, K., and Coauthors, 2009: GSMaP Passive Microwave Precipitation Retrieval Algorithm : Algorithm Description and Validation. *J. Meteorol. Soc. Japan*, **87A**, 119–136, https://doi.org/10.2151/jmsj.87A.119.

Ashouri, H., K. L. Hsu, S. Sorooshian, D. K. Braithwaite, K. R. Knapp, L. D. Cecil, B. R. Nelson, and O. P. Prat, 2015: PERSIANN-CDR: Daily precipitation climate data record from multisatellite observations for hydrological and climate studies. *Bull. Am. Meteorol. Soc.*, **96**, 69–83, https://doi.org/10.1175/BAMS-D-13-00068.1.

Banzon, V., T. M. Smith, C. Liu, and W. Hankins, 2016: A long-term record of blended satellite and in situ sea surface temperature for climate monitoring, modeling and environmental studies. *Earth Syst. Sci. Data Discuss.*, 1–13, https://doi.org/10.5194/essd-2015-44.

Bao, J., S. C. Sherwood, L. V. Alexander, and J. P. Evans, 2017: Future increases in extreme precipitation exceed observed scaling rates. *Nat. Clim. Chang.*, **7**, 128–132, https://doi.org/10.1038/nclimate3201.

Beck, H. E., A. I. J. M. van Dijk, V. Levizzani, J. Schellekens, D. G. Miralles, B. Martens, and A. de Roo, 2017: MSWEP: 3-hourly 0.25° global gridded precipitation (1979–2015) by merging gauge, satellite, and reanalysis data. *Hydrol. Earth Syst. Sci.*, **21**, 589–615, https://doi.org/10.5194/hess-21-589-2017.

Beck, H. E., E. F. Wood, M. Pan, C. K. Fisher, D. G. Miralles, A. I. J. M. Van Dijk, T. R. McVicar, and R. F. Adler, 2019: MSWep v2 Global 3-hourly 0.1° precipitation: Methodology and quantitative assessment. *Bull. Am. Meteorol. Soc.*, **100**, 473–500, https://doi.org/10.1175/BAMS-D-17-0138.1.

Bumke, K., R. P. Kedzierski, M. Schröder, C. Klepp, and K. Fennig, 2019: Validation of HOAPS rain retrievals against OceanRAIN In-situ measurements over the Atlantic Ocean. *Atmosphere (Basel).*, **10**,

https://doi.org/10.3390/atmos10010015.

Burdanowitz, J., S. A. Buehler, S. Bakan, and C. Klepp, 2019: On the sensitivity of oceanic precipitation to sea surface temperature. *Atmos. Chem. Phys. Discuss.*, **1**, 1–21, https://doi.org/10.5194/acp-2019-136.

Donlon, C. J., M. Martin, J. Stark, J. Roberts-Jones, E. Fiedler, and W. Wimmer, 2012: The Operational Sea Surface Temperature and Sea Ice Analysis (OSTIA) system. *Remote Sens. Environ.*, **116**, 140–158, https://doi.org/10.1016/j.rse.2010.10.017.

Fennig, K., M. Schröder, A. Andersson, and R. Hollmann, 2020: A Fundamental Climate Data Record of SMMR, SSM/I, and SSMIS brightness temperatures. *Earth Syst. Sci. Data*, **12**, 647–681, https://doi.org/10.5194/essd-12-647-2020.

Fischer, E. M., and R. Knutti, 2016: Observed heavy precipitation increase confirms theory and early models. *Nat. Clim. Chang.*, **6**, 986–991, https://doi.org/10.1038/nclimate3110.

Gentemann, C. L., F. J. Wentz, M. Brewer, K. Hilburn, and D. Smith, 2010: Passive microwave remote sensing of the ocean: An overview. *Oceanogr. from Sp. Revisit.*, 13–33, https://doi.org/10.1007/978-90-481-8681-5_2.

Gorman, P. A. O., and T. Schneider, 2009: The physical basis for increases in precipitation extremes in simulations of 21st-century climate change SCIENCES.

Gosset, M., M. Alcoba, R. Roca, S. Cloché, and G. Urbani, 2018: Evaluation of TAPEER daily estimates and other GPM-era products against dense gauge networks in West Africa, analysing ground reference uncertainty. *Q. J. R. Meteorol. Soc.*, **144**, 255–269, https://doi.org/10.1002/qj.3335.

592 Greene, J. S., M. Klatt, M. Morrissey, and S. Postawko, 2008: The comprehensive
593 pacific rainfall database. *J. Atmos. Ocean. Technol.*, **25**, 71–82,
594 https://doi.org/10.1175/2007JTECHA904.1.

595 Henderson, D. S., C. D. Kummerow, D. A. Marks, and W. Berg, 2017: A regime-
596 based evaluation of TRMM oceanic precipitation biases. *J. Atmos. Ocean.*
597 *Technol.*, **34**, 2613–2635, https://doi.org/10.1175/JTECH-D-16-0244.1.

598 Hong, Y., K. L. Hsu, S. Sorooshian, and X. Gao, 2004: Precipitation estimation from
599 remotely sensed imagery using an artificial neural network cloud classification
600 system. *J. Appl. Meteorol.*, **43**, 1834–1852, https://doi.org/10.1175/jam2173.1.

601 Huffman, G. J., and Coauthors, 1997: The Global Precipitation Climatology Project
602 (GPCP) Combined Precipitation Dataset. *Bull. Am. Meteorol. Soc.*, **78**, 5–20,
603 https://doi.org/10.1175/1520-0477(1997)078<0005:TGPCPG>2.0.CO;2.

604 ——, R. F. Adler, M. M. Morrissey, D. T. Bolvin, S. Curtis, R. Joyce, B. McGavock,
605 and J. Susskind, 2001: Global precipitation at one-degree daily resolution from
606 multisatellite observations. *J. Hydrometeorol.*, **2**, 36–50,
607 https://doi.org/10.1175/1525-7541(2001)002<0036:GPAODD>2.0.CO;2.

608 ——, and Coauthors, 2007: The TRMM Multisatellite Precipitation Analysis (TMPA):
609 Quasi-global, multiyear, combined-sensor precipitation estimates at fine scales.
610 *J. Hydrometeorol.*, **8**, 38–55, https://doi.org/10.1175/JHM560.1.

611 Huffman, G. J., R. F. Adler, D. T. Bolvin, and E. J. Nelkin, 2009: The TRMM Multi-
612 Satellite Precipitation Analysis (TMPA). *Satell. Rainfall Appl. Surf. Hydrol.*, 3–22,
613 https://doi.org/10.1007/978-90-481-2915-7_1.

614 ——, and Coauthors, 2018: Algorithm Theoretical Basis Document (ATBD) NASA

615 Global Precipitation Measurement (GPM) Integrated Multi-satellitE Retrievals
616 for GPM (IMERG) Prepared by :

617 Huffman, G. J., and Coauthors, 2020: Integrated Multi-satellite Retrievals for the
618 Global Precipitation Measurement (GPM) Mission (IMERG). 343–353,
619 https://doi.org/10.1007/978-3-030-24568-9_19.

620 Joyce, R. J., and P. Xie, 2011: Kalman Filter–Based CMORPH. *J. Hydrometeorol.*,
621 **12**, 1547–1563, https://doi.org/10.1175/JHM-D-11-022.1.

622 Khan, S., and V. Maggioni, 2019: Assessment of level-3 Gridded Global Precipitation
623 Mission (GPM) products over oceans. *Remote Sens.*, **11**, 255,
624 https://doi.org/10.3390/rs11030255.

625 Klepp, C., and Coauthors, 2018: OceanRAIN, a new in-situ shipboard global ocean
626 surface-reference dataset of all water cycle components. *Sci. Data*, **5**, 1–22,
627 https://doi.org/10.1038/sdata.2018.122.

628 Kubota, T., and Coauthors, 2020: Global Satellite Mapping of Precipitation (GSMaP)
629 Products in the GPM Era. *Satellite precipitation measurement*, V. Levizzani, C.
630 Kidd, D. Kirschbaum, C. Kummerow, K. Nakamura, and F.J. Turk, Eds.,
631 Springer, 355–373.

632 L'Ecuyer, T. S., and Coauthors, 2015: The observed state of the energy budget in the
633 early twenty-first century. *J. Clim.*, **28**, 8319–8346, https://doi.org/10.1175/JCLI-
634 D-14-00556.1.

635 Lafore, J. P., and Coauthors, 2016: Deep convection. *Meteorol. Trop. West Africa*
636 *Forecast. Handb.*, 90–129, https://doi.org/10.1002/9781118391297.ch3.

637 Levizzani, V., and Coauthors, 2018: The activities of the International Precipitation

638 Working Group. *Q. J. R. Meteorol. Soc.*, https://doi.org/10.1002/qj.3214.

639 Masunaga, H., M. Schröder, F. A. Furuzawa, C. Kummerow, E. Rustemeier, and U.
640 Schneider, 2019: Inter-product biases in global precipitation extremes. *Environ.*
641 *Res. Lett.*, **14**, 125016, https://doi.org/10.1088/1748-9326/ab5da9.

642 Muller, C. J., and Y. Takayabu, 2020: Response of precipitation extremes to
643 warming: what have we learned from theory and idealized cloud-resolving
644 simulations, and what remains to be learned? *Environ. Res. Lett.*,
645 https://doi.org/10.1088/1748-9326/ab7130.

646 Muller, C. J., P. A. O'Gorman, and L. E. Back, 2011: Intensification of precipitation
647 extremes with warming in a cloud-resolving model. *J. Clim.*, **24**, 2784–2800,
648 https://doi.org/10.1175/2011JCLI3876.1.

649 O'Gorman, P. A., 2015: Precipitation Extremes Under Climate Change. *Curr. Clim.*
650 *Chang. Reports*, **1**, 49–59, https://doi.org/10.1007/s40641-015-0009-3.

651 Pendergrass, A. G., 2020: Changing Degree of Convective Organization as a
652 Mechanism for Dynamic Changes in Extreme Precipitation. *Curr. Clim. Chang.*
653 *Reports*, **6**, 47–54, https://doi.org/10.1007/s40641-020-00157-9.

654 Prakash, S., and R. M. Gairola, 2014: Validation of TRMM-3B42 precipitation product
655 over the tropical Indian Ocean using rain gauge data from the RAMA buoy array.
656 *Theor. Appl. Climatol.*, **115**, 451–460, https://doi.org/10.1007/s00704-013-0903-
657 3.

658 ——, M. R. R. Kumar, S. Mathew, and R. Venkatesan, 2017: How accurate are
659 satellite estimates of precipitation over the north Indian Ocean ?

660 Rayner, N. A., D. E. Parker, E. B. Horton, C. K. Folland, L. V. Alexander, D. P.

Rowell, E. C. Kent, and A. Kaplan, 2003: Global analyses of sea surface temperature, sea ice, and night marine air temperature since the late nineteenth century. *J. Geophys. Res. D Atmos.*, **108**, https://doi.org/10.1029/2002jd002670.

Roca, R., 2019: Estimation of extreme daily precipitation thermodynamic scaling using gridded satellite precipitation products over tropical land. *Environ. Res. Lett.*, **14**, https://doi.org/10.1088/1748-9326/ab35c6.

——, and T. Fiolleau, 2020: Extreme precipitation in the tropics is closely associated with long-lived convective systems. *Commun. Earth Environ.*, **1**, 1–6, https://doi.org/10.1038/s43247-020-00015-4.

——, and Coauthors, 2018: Quantifying the contribution of the Megha-Tropiques mission to the estimation of daily accumulated rainfall in the Tropics. *Q. J. R. Meteorol. Soc.*, **144**, 49–63, https://doi.org/10.1002/qj.3327.

——, L. V. Alexander, G. Potter, M. Bador, R. Jucá, S. Contractor, M. G. Bosilovich, and S. Cloché, 2019: FROGs: a daily 1x1 gridded precipitation database of rain gauge, satellite and reanalysis products. *Earth Syst. Sci. Data*, 1017–1035, https://doi.org/10.5194/essd-11-1017-2019.

——, A. Guérou, R. A. Jucá Oliveira, P. Chambon, M. Gosset, S. Cloché, and M. Schröder, 2020: Merging the Infrared Fleet and the Microwave Constellation for Tropical Hydrometeorology (TAPEER) and Global Climate Monitoring (GIRAFE) Applications. 429–450.

Schär, C., and Coauthors, 2016: Percentile indices for assessing changes in heavy precipitation events. *Clim. Change*, **137**, 201–216, https://doi.org/10.1007/s10584-016-1669-2.

Serra, Y. L., 2018: Precipitation measurements from the Tropical Moored Array: A review and look ahead. *Q. J. R. Meteorol. Soc.*, **144**, 221–234, https://doi.org/10.1002/qj.3287.

Shige, S., and Coauthors, 2009: The GSMaP precipitation retrieval algorithm for microwave sounderspart i: Over-ocean algorithm. *IEEE Trans. Geosci. Remote Sens.*, **47**, 3084–3097, https://doi.org/10.1109/TGRS.2009.2019954.

Stephens, G. L., and T. D. Ellis, 2008: Controls of global-mean precipitation increases in global warming GCM experiments. *J. Clim.*, **21**, 6141–6155, https://doi.org/10.1175/2008JCLI2144.1.

——, J. M. Slingo, E. Rignot, J. T. Reager, M. Z. Hakuba, P. J. Durack, J. Worden, and R. Rocca, 2020: Earth's water reservoirs in a changing climate. *Proc. R. Soc. A Math. Phys. Eng. Sci.*, **476**, https://doi.org/10.1098/rspa.2019.0458.

Sun, Q., C. Miao, Q. Duan, H. Ashouri, S. Sorooshian, and K. L. Hsu, 2018: A Review of Global Precipitation Data Sets: Data Sources, Estimation, and Intercomparisons. *Rev. Geophys.*, **56**, 79–107, https://doi.org/10.1002/2017RG000574.

Tan, J., G. J. Huffman, D. T. Bolvin, and E. J. Nelkin, 2019: Diurnal Cycle of IMERG V06 Precipitation. *Geophys. Res. Lett.*, **46**, 13584–13592, https://doi.org/10.1029/2019GL085395.

Trenberth, K. E., 1999: Conceptual framework for changes of extremes of the hydrological cycle with climate change. *Clim. Change*, **42**, 327–339, https://doi.org/10.1023/A:1005488920935.

USHIO, T., and Coauthors, 2009: A Kalman Filter Approach to the Global Satellite

Mapping of Precipitation (GSMaP) from Combined Passive Microwave and Infrared Radiometric Data. *J. Meteorol. Soc. Japan*, **87A**, 137–151, https://doi.org/10.2151/jmsj.87a.137.

Wentz, F. J., C. Gentemann, D. Smith, and D. Chelton, 2000: Satellite measurements of sea surface temperature through clouds. *Science (80-.).*, **288**, 847–850, https://doi.org/10.1126/science.288.5467.847.

Westra, S., and Coauthors, 2014: Future changes to the intensity and frequency of short-duration extreme rainfall. *Rev. Geophys.*, **52**, 522–555, https://doi.org/10.1002/2014RG000464.

Wu, Q., and Y. Wang, 2019: Comparison of oceanic multisatellite precipitation data from tropical rainfall measurement mission and global precipitation measurement mission datasets with rain gauge data from ocean buoys. *J. Atmos. Ocean. Technol.*, **36**, 903–920, https://doi.org/10.1175/JTECH-D-18-0152.1.

Xie, P., R. Joyce, S. Wu, S. H. Yoo, Y. Yarosh, F. Sun, and R. Lin, 2017: Reprocessed, bias-corrected CMORPH global high-resolution precipitation estimates from 1998. *J. Hydrometeorol.*, **18**, 1617–1641, https://doi.org/10.1175/JHM-D-16-0168.1.

Zhang, X., L. Alexander, G. C. Hegerl, P. Jones, A. K. Tank, T. C. Peterson, B. Trewin, and F. W. Zwiers, 2011: Indices for monitoring changes in extremes based on daily temperature and precipitation data. *Wiley Interdiscip. Rev. Clim. Chang.*, **2**, 851–870, https://doi.org/10.1002/wcc.147.

TABLES

Product shortname	Product name and version	Period used	Use of IR satellite data	Use of MW satellite data	Constellation based products	References
GSMaP	GSMaP-NRT-no gauges v6.0	2001-2017	Yes	Yes	Yes	Kubota et al. (2009)
CMORPH	CMORPH V1.0 CRT	2001-2017	Yes	Yes	Yes	Xie et al. (2017)
MSWE	MSWEP 2.2	2001-10.2017	Yes	Yes	Yes	Beck et al. (2017)
TMPA	3B42 v7.0	2001-2017	Yes	Yes	Yes	Huffman et al. (2009)
HOAPS	HOAPS	2001-2016	Yes	Yes	Yes	Anderson et al. (2014)
IMERG	IMERG V06 final run	2001-2017	Yes	Yes	Yes	Huffman et al. (2018)
PERSIANN	PERSIANN CDR v1	2001-2017	Yes	No	No	Ashouri et al. (2015)
GPCP	GPCP 1DD v1.3 CRD	2001-2017	Yes	Yes	No	Huffman et al. (2001)
TAPEER	TAPEER-BRAIN v1.5	2012-2016	Yes	Yes	Yes	Roca et al. (2020)

Table 1: List of gridded precipitation products and their acronyms. Note that the MWSEP v2.2 data have been acquired directly from H. Beck. The constellation products are using multiple microwave platforms.

Product shortname	Product name and version	Use of satellite data	Period used	References
OSTIA	OSTIA Near Real Time Level 4 SST	IR + MW	2007-2017	Donlon et al. (2012)
OISST	NOAA CDR OISST AVHRR-only v2	IR	2001-2007	Reynolds et al. (2008)
OIRSS	RSS OI SST MW v5	MW	2001-2017	Gentemann et al. (2010)

Table 2: List of sea surface temperature products and their acronyms. IR stands for Infra-red and MW for Microwave.

a.

Products	OSTIA 2007-2017 T(t) 58%	OSTIA 2007-2017 T(t-24h) 56%	OSTIA 2007-2017 T(t-48h) 55%	OSTIA 2012-2016 T(t) 57%	OSTIA 2012-2016 T(t-24h) 56%	OSTIA 2012-2016 T(t-48h) 54%
GSMaP	4.21	5.37	5.38	5.43	6.09	6
CMORPH	5.26	6.02	6.11	5.74	6.21	6.7
MSWEP	4.69	5.61	5.52	5.89	6.69	6.77
TMPA	5.09	5.51	5.75	4.93	5.29	5.61
HOAPS	5.75	7.14	7.05	5.76	6.82	6.9
IMERG	5.19	5.81	5.5	4.85	5.24	5.24
ENS	5.04	5.95	5.9	5.41	6.05	6.17
Mean ENS	**5.03**	**5.91**	**5.89**	**5.43**	**6.06**	**6.2**
STD ENS	0.52	0.65	0.62	0.45	0.67	0.69
Cvar ENS	10.43	10.93	10.62	8.26	11.1	11.09

Table 3.a: Summary of the sensibility analysis with the value of the slope of the 99.9th percentile as a function of the SST from the OSTIA product over the CC regime ([300K,302,5K[) in %.K^{-1}. Mean (%.K^{-1}), standard deviation (%.K^{-1}) and coefficient of variation (%) for the ensemble of all the products (ENS), as well as the total rainfall accumulation within the regime, are also reported.

b.

Products	OISST 2007-2017 T(t) 58%	OISST 2007-2017 T(t-24h) 57%	OISST 2007-2017 T(t-48h) 57%	OISST 2012-2016 T(t) 56%	OISST 2012-2016 T(t-24h) 55%	OISST 2012-2016 T(t-48h) 54%	OISST 2001-2017 T(t) 60%	OISST 2001-2017 T(t-24h) 59%	OISST 2001-2017 T(t-48h) 58%
GSMaP	2.64	4.88	6.08	4.27	5.69	6.91	2.78	4.02	4.54
CMORPH	3.15	4.89	5.37	4.34	5.7	6.4	1.07	1.97	2.42
MSWEP	3.35	5.52	6.03	4.87	6.83	7.54	3.08	4.46	4.7
TMPA	3.68	5.1	5.44	4.98	5.73	5.88	3.11	4.2	4.47
HOAPS	4.5	6.1	7.06	5.19	6.67	7.86	4.18	5	5.58
IMERG	3.21	4.84	5.43	3.88	5.7	6.21	2.92	3.93	4.37
ENS	3.43	5.23	5.95	4.56	6.06	6.84	2.96	4.02	4.46
Mean ENS	**3.42**	**5.22**	**5.9**	**4.59**	**6.05**	**6.8**	**2.86**	**3.93**	**4.35**
STD ENS	0.63	0.5	0.65	0.5	0.54	0.78	1.01	1.04	1.04
Cvar ENS	18.27	9.6	10.99	10.89	8.95	11.48	35.26	26.35	23.94

Table 3.b: Summary of the sensibility analysis with the value of the slope of the 99.9th percentile as a function of the SST from the OISST product over the CC regime ([300K,302,5K[) in %.K^{-1}. Mean (%.K^{-1}), standard deviation (%.K^{-1}) and coefficient of variation (%) for the ensemble of all the products (ENS), as well as the total rainfall accumulation within the regime, are also reported.

c.

Products	OIRSS 2007-2017 T(t) 60%	OIRSS 2007-2017 T(t-24h) 58%	OIRSS 2007-2017 T(t-48h) 57%	OIRSS 2012-2016 T(t) 58%	OIRSS 2012-2016 T(t-24h) 56%	OIRSS 2012-2016 T(t-48h) 55%	OIRSS 2001-2017 T(t) 61%	OIRSS 2001-2017 T(t-24h) 59%	OIRSS 2001-2017 T(t-48h) 59%
GSMaP	-1.54	3.76	5.43	-0.6	3.76	5.07	-2.09	3.01	4.54
CMORPH	-0.19	4.59	6.82	-0.83	4.8	7.01	-2.82	2.2	4.38
MSWEP	-1.56	4.1	6.05	-1.02	4.9	6.64	-2.39	3.22	5.3
TMPA	2.26	5.46	6.27	1.85	5.21	5.91	1.2	5.37	6.5
HOAPS	-0.65	4.23	6.36	-1.3	3.79	6.33	-1.14	3.96	5.78
IMERG	-1.03	4.05	5.1	-1.03	3.77	4.91	-0.88	3.99	5.51
ENS	-0.61	4.28	5.9	-0.62	4.25	5.86	-1.34	3.65	5.34
Mean ENS	**-0.45**	**4.36**	**6**	**-0.49**	**4.37**	**5.98**	**-1.35**	**3.63**	**5.34**
STD ENS	1.43	0.6	0.63	1.17	0.67	0.85	1.45	1.08	0.79
Cvar ENS	-316.64	13.73	10.54	-239.42	15.31	14.19	-107.5	29.81	14.86

Table 3.c: Summary of the sensibility analysis with the value of the slope of the 99.9th percentile as a function of the SST from the OIRSS product over the CC regime ([300K,302,5K[) in %.K^{-1}. Mean (%.K^{-1}), standard deviation (%.K^{-1}) and coefficient of variation (%) for the ensemble of all the products (ENS), as well as the total rainfall accumulation within the regime, are also reported.

FIGURES

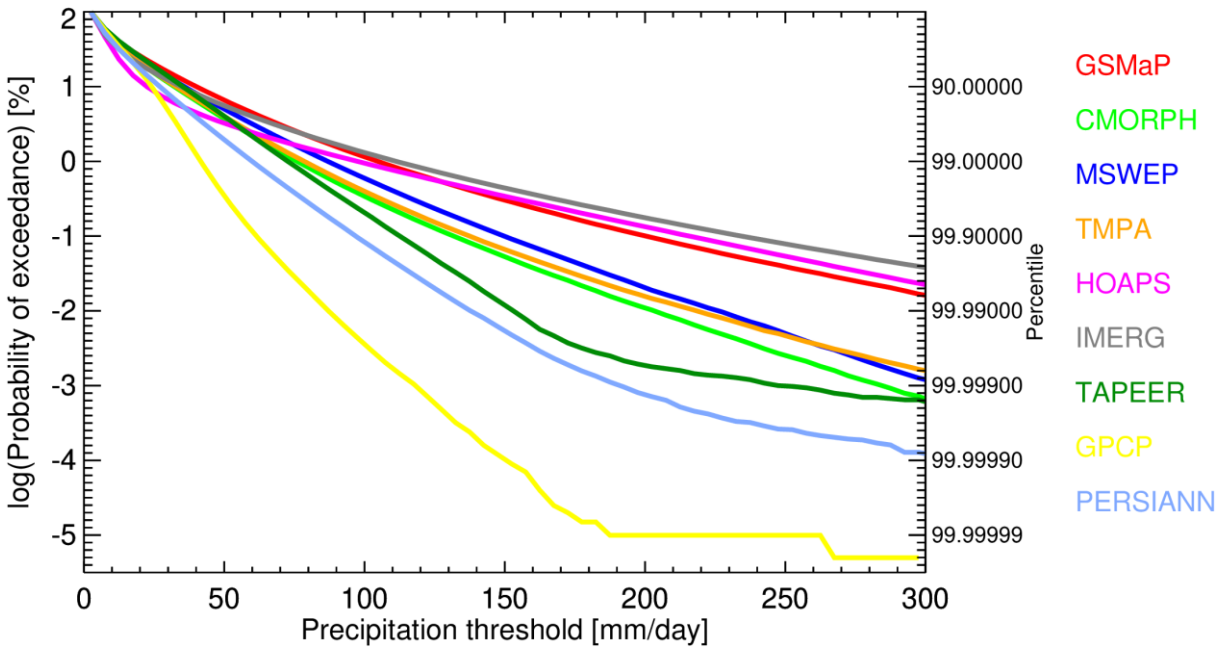

Figure 1: Probability of exceedance of daily 1°x1° accumulated precipitation over the tropical ocean (30°S-30°N) for the period 2017-2017 except for the TAPEER product where it is restricted to the 2012-2016 period. The probability of exceedance is computed with respect to wet-days with precipitation above 1mm/d.

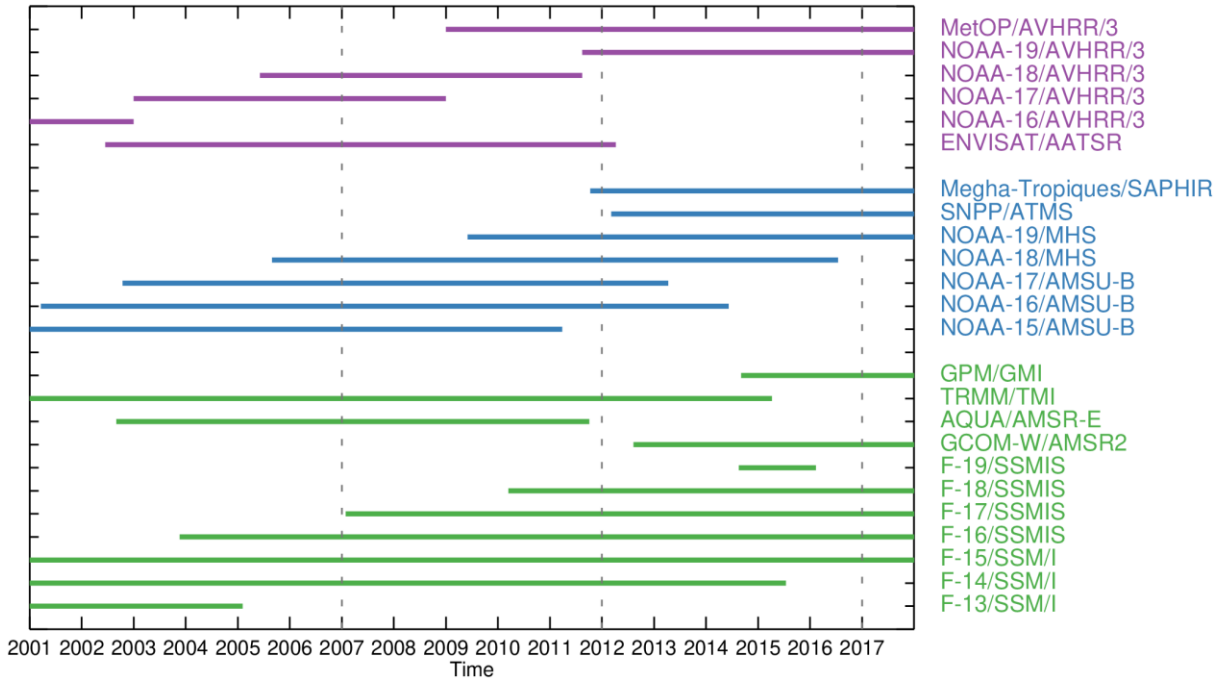

Figure 2: Time series of the availability of microwave imagers and sounders used in the precipitation products of the study. Vertical dashed lines indicate the different time periods explored in the study.

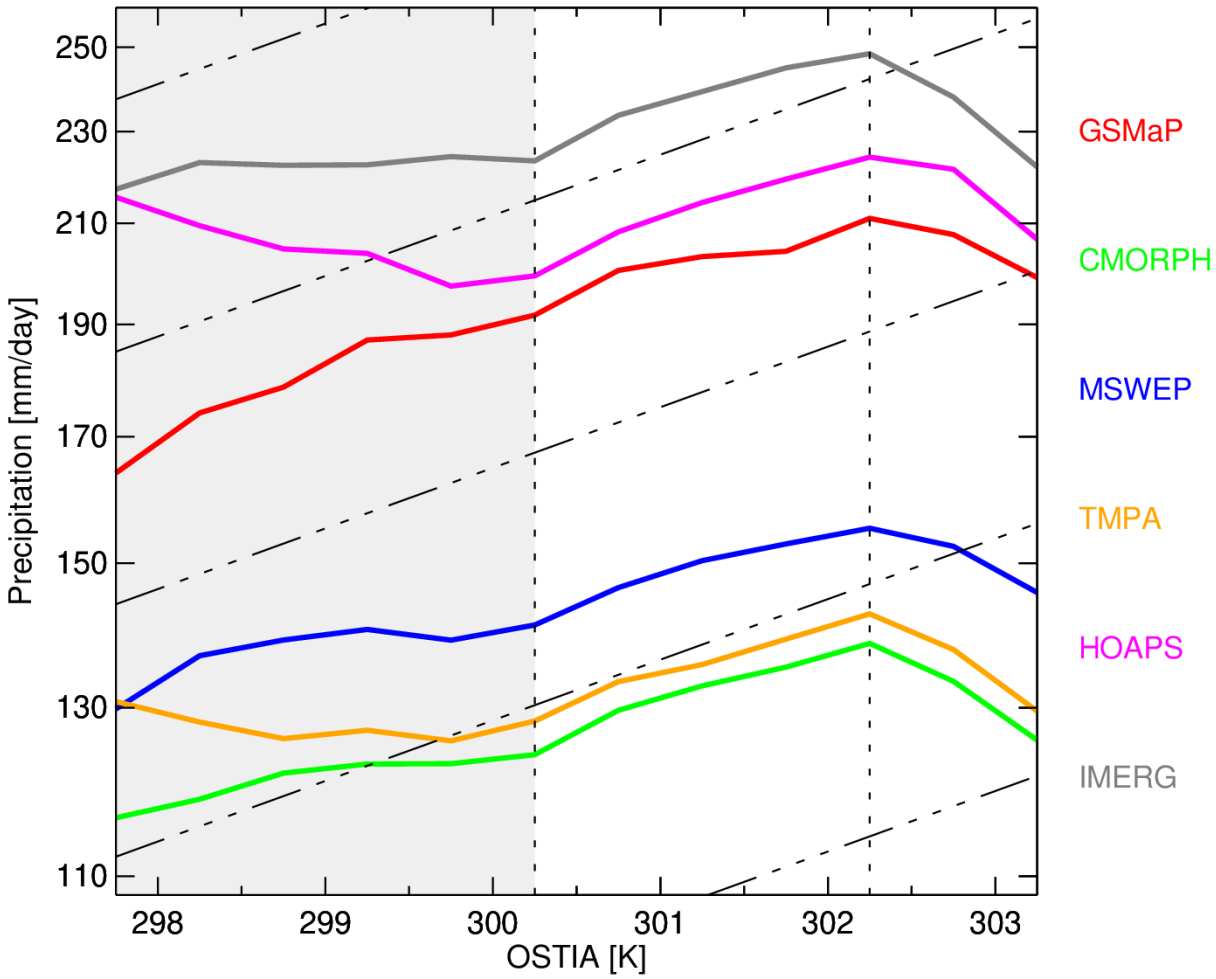

Figure 3: The value of the 99.9th percentile of the 1°x1° daily accumulated precipitation as a function of the contemporaneous SST from the OSTIA product. Each color corresponds to a precipitation product. For the period 2007-2017. Regimes are separated by vertical dashed lines. The grey shaded area indicates the non-robust cold regime between precipitation products. Black dash-dotted lines correspond to the Clausius-Clapeyron 6%K^{-1} rate. See text for details.

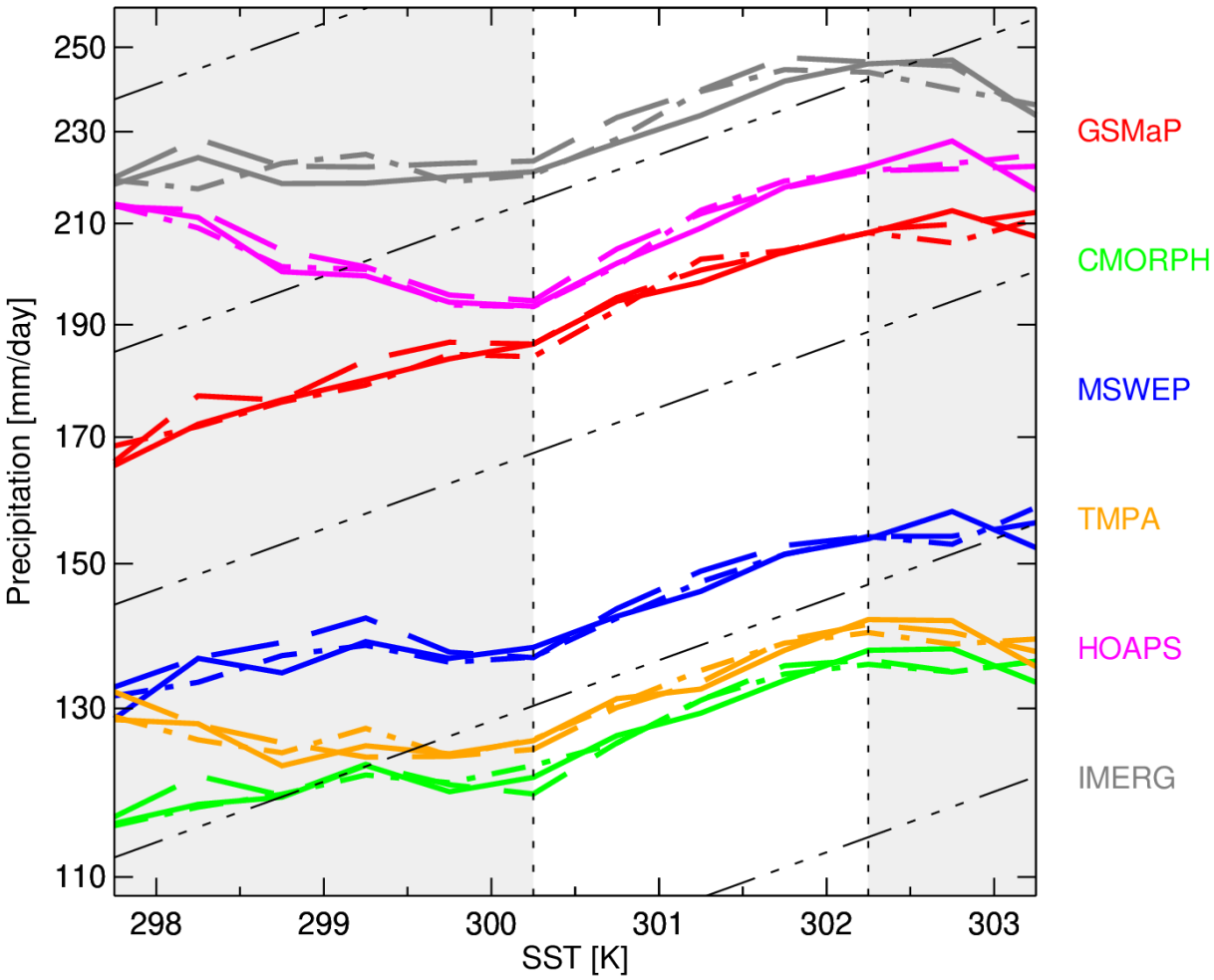

Figure 4: The value of the 99.9th percentile of the 1°x1° daily accumulated precipitation as a function of the SST lagged by 2 days. Each color corresponds to a precipitation product. Solid line for OSTIA, dashed line for OISST and dash-dotted lines for OIRSS. For the period 2007-2017. Regimes are separated by vertical dashed lines. The grey shaded areas indicate the non-robust cold regime between precipitation products (left) and the non-robust warm regime between SST products (right). Black dash-dotted lines correspond to the Clausius-Clapeyron 6%K^{-1} rate. See text for details.

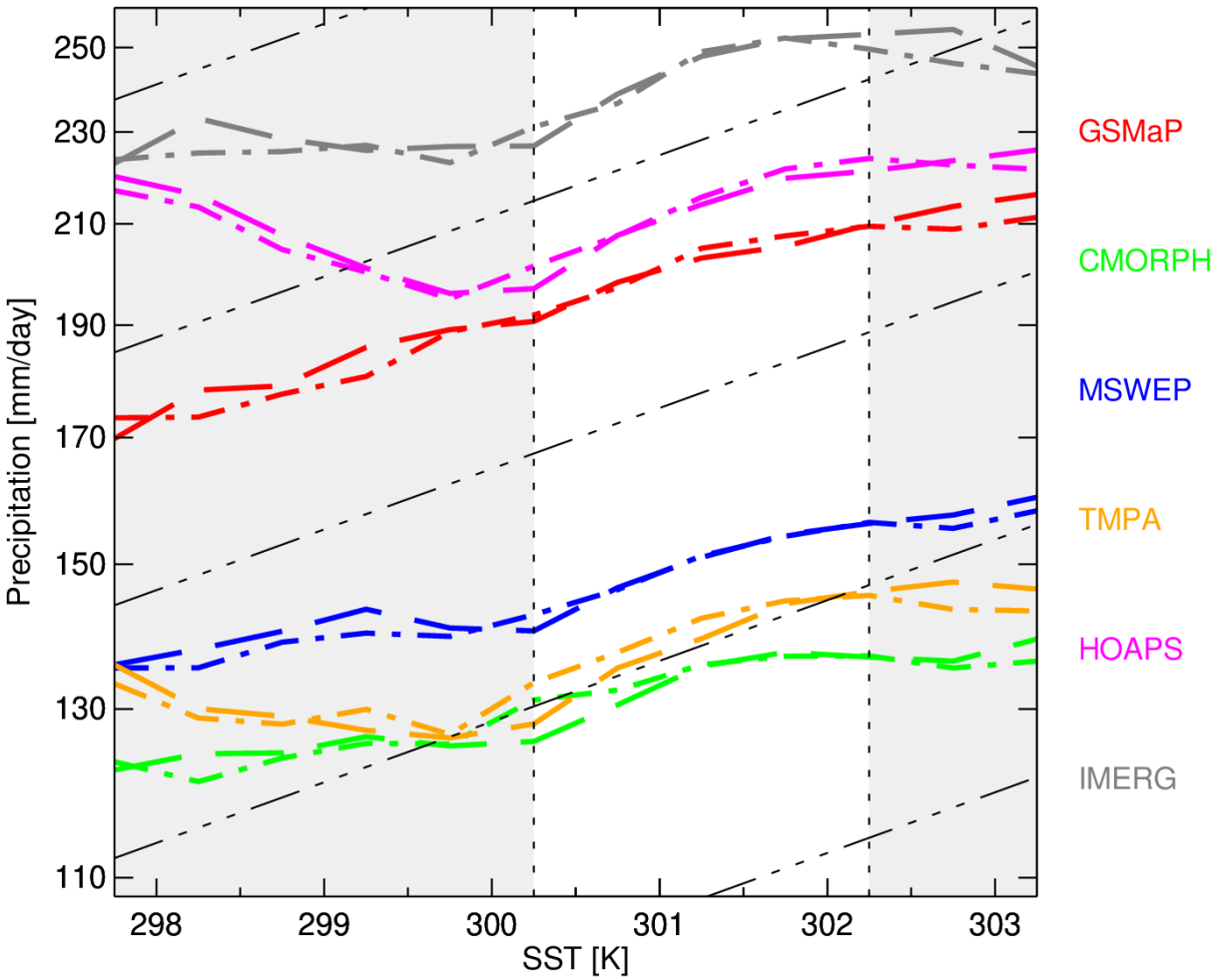

Figure 5: The value of the 99.9th percentile of the 1°x1° daily accumulated precipitation as a function of the SST lagged by 2 days. Each color corresponds to a precipitation product. Dashed line for OISST and dash-dotted lines for OIRSS. For the period 2001-2017. Regimes are separated by vertical dashed lines. The grey shaded areas indicate the non-robust cold regime between precipitation products (left) and the non-robust warm regime between SST products (right). Black dash-dotted lines correspond to the Clausius-Clapeyron 6%K^{-1} rate. See text for details.

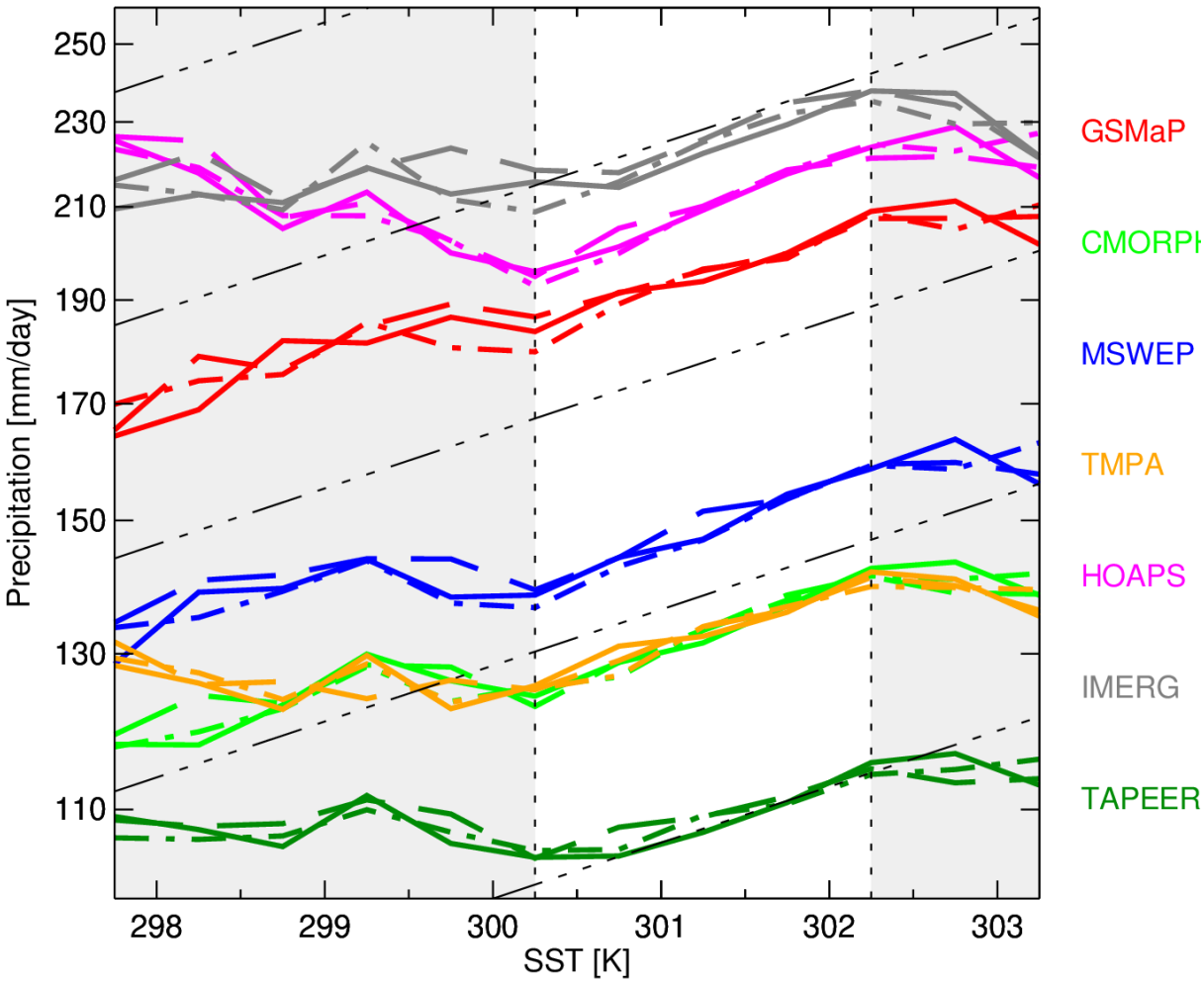

Figure 6 : The value of the 99.9th percentile of the 1°x1° daily accumulated precipitation as a function of the SST lagged by 2 days. Each color corresponds to a precipitation product. Solid line for OSTIA, dashed line for OISST and dash-dotted lines for OIRSS. For the period 2012-2016. Regimes are separated by vertical dashed lines. The grey shaded areas indicate the non-robust cold regime between precipitation products (left) and the non-robust warm regime between SST products (right). Black dash-dotted lines correspond to the Clausius-Clapeyron 6%K^{-1} rate. See text for details.

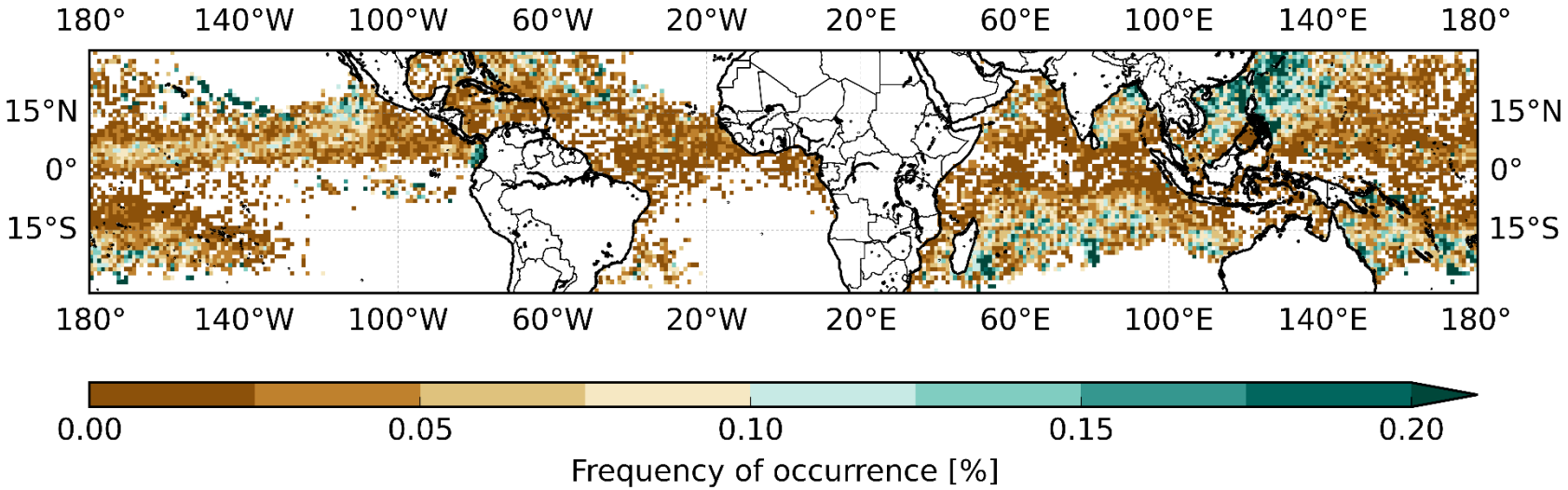

Figure 7: Map of the ensemble mean frequency of occurrence (%) of precipitation greater than the percentile 99.9th for the CC SST regime ([300 K; 302.5 K]). SST from OSTIA over the period 2007-2017, lagged by 2 days, are used to delineate the regime.